Robustness of cosmological axion mass limits

Eleonora Di Valentino, Stefano Gariazzo, Elena Giusarma, Olga Mena

PHYSICAL REVIEW D **91,** 123505 (2015)

Robustness of cosmological axion mass limits

Eleonora Di Valentino,[1,2] Stefano Gariazzo,[3,4] Elena Giusarma,[5] and Olga Mena[6]
[1]*CNRS, UMR 7095, Institut d'Astrophysique de Paris, F-75014, Paris, France*
[2]*Sorbonne Universités, Institut Lagrange de Paris (ILP), F-75014, Paris, France*
[3]*Department of Physics, University of Torino, Via P. Giuria 1, I–10125 Torino, Italy*
[4]*INFN, Sezione di Torino, Via P. Giuria 1, I–10125 Torino, Italy*
[5]*Physics Department and INFN, Università di Roma "La Sapienza", Ple Aldo Moro 2, 00185, Rome, Italy*
[6]*IFIC, Universidad de Valencia-CSIC, 46071, Valencia, Spain*
(Received 9 March 2015; revised manuscript received 7 May 2015; published 4 June 2015)

We present the cosmological bounds on the thermal axion mass in an extended cosmological scenario in which the primordial power spectrum of scalar perturbations differs from the usual power-law shape predicted by the simplest inflationary models. The power spectrum is instead modeled by means of a "piecewise cubic Hermite interpolating polynomial" (PCHIP). When using cosmic microwave background measurements combined with other cosmological data sets, the thermal axion mass constraints are degraded only slightly. The addition of the measurements of σ_8 and Ω_m from the 2013 Planck cluster catalog on galaxy number counts relaxes the bounds on the thermal axion mass, mildly favoring a $\sim$1 eV axion mass, regardless of the model adopted for the primordial power spectrum. However, in general, such a preference disappears if the sum of the three active neutrino masses is also considered as a free parameter in our numerical analyses, due to the strong correlation between the masses of these two hot thermal relics.

DOI: 10.1103/PhysRevD.91.123505 PACS numbers: 98.80.-k, 95.85.Sz, 98.70.Vc, 98.80.Cq

I. INTRODUCTION

A possible candidate for an extra hot thermal relic component is the axion particle produced thermally in the early Universe. Axions therefore can contribute to the hot dark matter component together with the standard relic neutrino background. Axions may be produced in the early Universe via thermal or nonthermal processes, and arise as the solution to solve the strong CP problem [1–3]. Axions are the pseudo-Nambu-Goldstone bosons of a new global $U(1)_{\rm PQ}$ (Peccei-Quinn) symmetry that is spontaneously broken at an energy scale f_a. The axion mass is given by

$$m_a = \frac{f_\pi m_\pi}{f_a}\frac{\sqrt{R}}{1+R} = 0.6\ \text{eV}\frac{10^7\ \text{GeV}}{f_a}, \qquad (1)$$

where f_a is the axion coupling constant, $R = 0.553 \pm 0.043$ is the up-to-down quark masses ratio, and $f_\pi = 93$ MeV is the pion decay constant. Nonthermal axions such as those produced by the misalignment mechanism, while being a negligible hot dark matter candidate, may constitute a fraction or the total cold dark matter component of the Universe. We do not explore such a possibility here. Thermal axions will affect the cosmological observables in a very similar way to that induced by the presence of neutrino masses and/or extra sterile neutrino species. Massive thermal axions such as hot relics affect large-scale structure, since they will only cluster at scales larger than their free-streaming scale when they become nonrelativistic, suppressing therefore structure formation at small scales (large wave numbers k). Concerning cosmic microwave background (CMB) physics, an axion mass will also lead to a signature in the CMB photon temperature anisotropies via the early integrated Sachs-Wolfe effect. In addition, extra light species such as thermal axions will contribute to the dark radiation content of the Universe, or, in other words, will lead to an increase in the effective number of relativistic degrees of freedom $N_{\rm eff}$, defined via

$$\rho_{\rm rad} = \left[1 + \frac{7}{8}\left(\frac{4}{11}\right)^{4/3} N_{\rm eff}\right]\rho_\gamma, \qquad (2)$$

where ρ_γ refers to the present photon energy density. In the standard cosmological model in which a thermal axion content is absent, the three active neutrino contribution leads to the canonical value of $N_{\rm eff} = 3.046$ [4]. The extra contribution to $N_{\rm eff}$ arising from thermal axions can modify both the CMB anisotropies (via Silk damping) and the light element primordial abundances predicted by big bang nucleosynthesis. The former cosmological signatures of thermal axions have been extensively exploited in the literature to derive bounds on the thermal axion mass; see Refs. [5–10].

However, all the cosmological axion mass limits to date have assumed the usual simple power-law description for the primordial perturbations. The aim of this paper is to constrain the mass of the thermal axion using a nonparametric description of the primordial power spectrum (PPS hereinafter) of the scalar perturbations, as introduced in Ref. [11]. While in the simplest models of inflation [12–22] the PPS has a scale-free power-law form, the PPS could be more complicated, presenting various features or a

scale dependence. Several methods have been proposed in the literature to reconstruct the shape of the PPS (see the recent work of Ref. [23]). It has been shown [24,25] that there are small hints for deviations from the power-law form, even when using different methods and different data sets.

The energy scales at which the PPS was produced during inflation cannot be directly tested. We can only infer the PPS by measuring the current matter power spectrum in the galaxy distribution and the power spectrum of the CMB fluctuations. The latter one, measured with exquisite precision by the Planck experiment [26–28], is the convolution of the PPS with the transfer function. Therefore, in order to reconstruct the PPS, the assumption of an underlying cosmological model is a mandatory first step in order to compute the transfer function.

Here we rather exploit a nonstandard PPS approach, which can allow for a good fit to experimental data even in models that deviates from the standard cosmological picture. In particular, we consider a thermal axion scenario, allowing the PPS to assume a more general shape than the usual power-law description. This will allow us to test the robustness of the cosmological thermal axion mass bounds (see Ref. [10] for a recent standard thermal axion analysis), as first performed in Ref. [29] for the neutrino mass case.

The structure of the paper is as follows. Section II describes the PPS modeling used in this study, as well as the description of the thermal axion model explored here and the cosmological data sets exploited to constrain such a model. In Sec. III we present and discuss the results arising from our Bayesian analysis, performed through the Monte Carlo Markov chains (MCMC) package `CosmoMC` [30], while the calculation of the theoretical observables is done through the Boltzman equations solver CAMB (Code for Anisotropies in the Microwave Background) [31]. We draw our conclusions in Sec. IV.

II. METHOD

In this section we focus on the tools used in the numerical analyses performed here. Subsection II A describes the alternative model for the PPS of scalar perturbations used for the analyses here (see also Ref. [11]), while in subsection II B we introduce the cosmological model and the thermal axion treatment followed in this study. Finally, we present in subsection II C the cosmological data sets used in the MCMC analyses.

A. Primordial power spectrum model

The primordial fluctuations in scalar and tensor modes are generated during the inflationary phase in the early Universe. The simplest models of inflation predict a power-law form for the PPS of scalar and tensor perturbations (see e.g. [12–22] and references therein), but in principle inflation can be generated by more complicated mechanisms, thus giving a different shape for the PPS (see Refs. [32,33] and references therein). In order to study how the cosmological constraints on the parameters change in more general inflationary scenarios, we assume a nonparametric form for the PPS.

Among the large number of possibilities, we decided to describe the PPS of scalar perturbations using a function to interpolate the PPS values in a series of nodes at fixed position. The interpolating function we used is named "piecewise cubic Hermite interpolating polynomial" (PCHIP) [34] and it is a modified spline function, defined to preserve the original monotonicity of the point series that is interpolated. We use a modified version of the original PCHIP algorithm [35], detailed in Appendix A of Ref. [11].

To describe the scalar PPS with the PCHIP model, we only need to give the values of the PPS in a discrete number of nodes and to interpolate among them. We use 12 nodes which span a wide range of k values:

$$\begin{aligned} k_1 &= 5 \times 10^{-6}\ \mathrm{Mpc}^{-1}, \\ k_2 &= 10^{-3}\ \mathrm{Mpc}^{-1}, \\ k_j &= k_2 (k_{11}/k_2)^{(j-2)/9} \quad \text{for } j \in [3, 10], \\ k_{11} &= 0.35\ \mathrm{Mpc}^{-1}, \\ k_{12} &= 10\ \mathrm{Mpc}^{-1}. \end{aligned} \tag{3}$$

We choose equally spaced nodes in the logarithmic scale in the range (k_2, k_{11}), that is well constrained from the data [29], while the first and the last nodes are useful to allow for a nonconstant behavior of the PPS outside the well-constrained range.

The PCHIP PPS is described by

$$P_s(k) = P_0 \times \mathtt{PCHIP}(k; P_{s,1}, \ldots, P_{s,12}), \tag{4}$$

where $P_{s,j}$ is the value of the PPS at the node k_j divided by $P_0 = 2.36 \times 10^{-9}$ [36].

B. Cosmological and axion model

The baseline scenario we consider here is the ΛCDM model, extended with hot thermal relics (the axions), together with the PPS approach outlined in the previous section. For the numerical analyses we use the following set of parameters, for which we assume flat priors in the intervals listed in Table I:

$$\left\{\omega_b, \omega_c, \Theta_s, \tau, m_a, \sum m_\nu, P_{s,1}, \ldots, P_{s,12}\right\}, \tag{5}$$

where $\omega_b \equiv \Omega_b h^2$ and $\omega_c \equiv \Omega_c h^2$ are, respectively, the physical baryon and cold dark matter energy densities, Θ_s is the ratio between the sound horizon and the angular diameter distance at decoupling, τ is the reionization optical depth, m_a and $\sum m_\nu$ are the axion and the sum of three active neutrino masses (both in eV), and $P_{s,1}, \ldots, P_{s,12}$ are

TABLE I. Priors for the parameters used in the MCMC analyses.

Parameter	Prior
$\Omega_b h^2$	[0.005, 0.1]
$\Omega_{cdm} h^2$	[0.001, 0.99]
Θ_s	[0.5, 10]
τ	[0.01, 0.8]
m_a (eV)	[0.1, 3]
$\sum m_\nu$ (eV)	[0.06, 3]
$P_{s,1}, \ldots, P_{s,12}$	[0.01, 10]
n_s	[0.9, 1.1]
$\log[10^{10} A_s]$	[2.7, 4]

the parameters of the PCHIP PPS. We shall also consider a scenario in which massive neutrinos are present, to explore the expected degeneracy between the sum of the neutrino masses and the thermal axion mass [10].

In order to compare the results obtained with the PCHIP PPS to the results obtained with the usual power-law PPS model, we describe the latter case with the following set of parameters:

$$\{\omega_b, \omega_c, \Theta_s, \tau, m_a, n_s, \log[10^{10} A_s]\}, \tag{6}$$

where n_s is the scalar spectral index, A_s the amplitude of the primordial spectrum, and the other parameters are the same ones described above. The case of several hot thermal relics for the standard scenario will not be carried out here, as it has been done in the past by several authors (see e.g. [10]). The flat priors we use are listed in Table I.

Concerning the contribution of the axion mass-energy density to the Universe's expansion rate, we briefly summarize our treatment in the following. Axions decoupled in the early Universe at a temperature T_D given by the usual freeze-out condition for a thermal relic:

$$\Gamma(T_D) = H(T_D), \tag{7}$$

where the thermally averaged interaction rate Γ refers to the $\pi + \pi \to \pi + a$ process:

$$\Gamma = \frac{3}{1024\pi^5} \frac{1}{f_a^2 f_\pi^2} C_{a\pi}^2 I_a, \tag{8}$$

with $C_{a\pi} = \frac{1-R}{3(1+R)}$ representing the axion-pion coupling constant and the integral I_a reads as follows

$$I_a = n_a^{-1} T^8 \int dx_1 dx_2 \frac{x_1^2 x_2^2}{y_1 y_2} f(y_1) f(y_2) \times \int_{-1}^{1} d\omega \frac{(s - m_\pi^2)^3 (5s - 2m_\pi^2)}{s^2 T^4}, \tag{9}$$

in which $n_a = (\zeta_3/\pi^2) T^3$ refers to the number density for axions in thermal equilibrium. The function $f(y) = 1/(e^y - 1)$ is the pion thermal distribution and there are three different kinematical variables $[x_i = |\vec{p}_i|/T$, $y_i = E_i/T$ $(i = 1, 2)$ and $s = 2(m_\pi^2 + T^2(y_1 y_2 - x_1 x_2 \omega))]$.

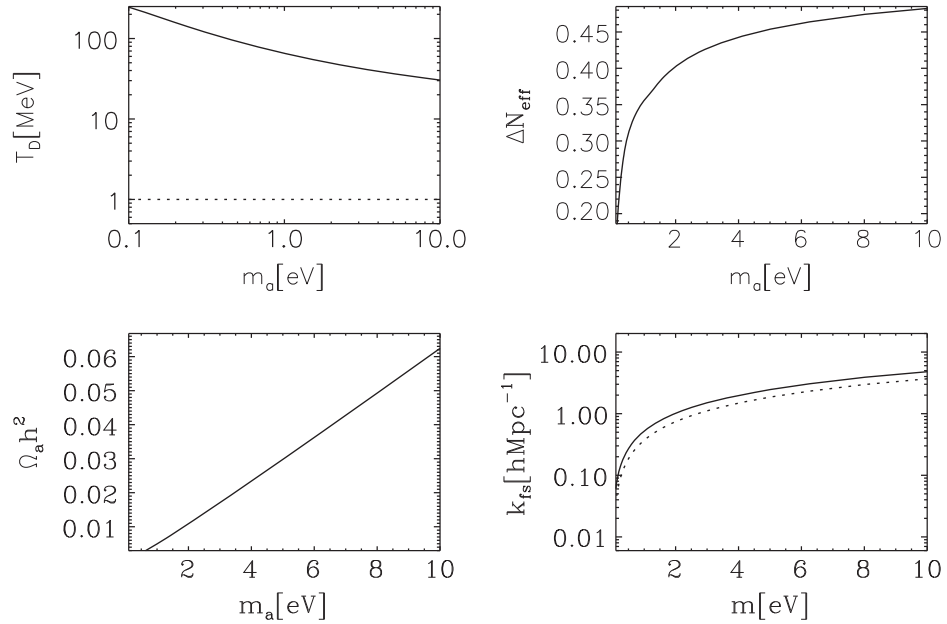

FIG. 1. The left upper panel shows the temperature of decoupling as a function of the axion mass (solid curve), as well as the big bang nucleosynthesis temperature, $T_{BBN} \simeq 1$ MeV (dashed curve). The right upper panel shows the axion contribution to the extra dark radiation content of the Universe, while the bottom right plot depicts the free-streaming scale of an axion (solid curve) or a neutrino (dashed curve) versus the axion/neutrino mass, in eV. The left bottom panel shows the current axion mass-energy density as a function of the axion mass.

The freeze-out equation above, Eq. (7), can be numerically solved, obtaining the axion decoupling temperature T_D as a function of the axion mass m_a. Figure 1 shows, in the left upper panel, the axion decoupling temperature as a function of the axion mass, in eV units. Notice that the higher the axion mass, the lower the temperature of decoupling. From the axion decoupling temperature, it is possible to infer the present axion number density, related to the current photon density n_γ by

$$n_a = \frac{g_{\star S}(T_0)}{g_{\star S}(T_D)} \times \frac{n_\gamma}{2}, \tag{10}$$

where $g_{\star S}$ represents the number of *entropic* degrees of freedom, with $g_{\star S}(T_0) = 3.91$. The contribution of the relic axion to the total mass-energy density of the Universe will be given by the product of the axion mass times the axion number density. The quantity $\Omega_a h^2$ at the present epoch is depicted in the bottom left panel of Fig. 1. Notice that, currently, a 1 eV axion will give rise to $\Omega_a h^2 \simeq 0.005$, while a neutrino of the same mass will contribute to the total mass-energy density of the Universe with $\Omega_\nu h^2 \simeq 0.01$. Notice, however, that $\Omega_a h^2$ represents the contribution from relic, thermal axion states. Nonthermal processes, such as the misalignment production, could also produce a nonthermal axion population which we do not consider here; see the work of [37] for the most recent cosmological constraints on such a scenario. As previously stated, the presence of a thermal axion will also imply an extra radiation component at the BBN period:

$$\Delta N_{\rm eff} = \frac{4}{7}\left(\frac{3}{2}\frac{n_a}{n_\nu}\right)^{4/3}, \tag{11}$$

where n_a is given by Eq. (10) and n_ν refers to the present neutrino plus antineutrino number density per flavor. The top right panel of Fig. 1 shows the axion contribution to the radiation component of the Universe as a function of the axion mass. Notice that the extra dark radiation arising from a 1 eV axion is still compatible (at 95% C.L.) with the most recent measurements of $N_{\rm eff}$ from the Planck mission [26]. The last crucial cosmological axion quantity is the axion free streaming scale, i.e. the wave number $k_{\rm fs}$ below which axion density perturbations will contribute to clustering once the axion is a nonrelativistic particle. This scale is illustrated in Fig. 1, in the bottom right panel, together with that corresponding to a neutrino of the same mass. Notice that they cover the same scales for our choice of priors for m_a and $\sum m_\nu$ and therefore one can expect a large correlation between these two quantities in measurements of galaxy clustering. We will explore this degeneracy in the following sections. We summarize the axion parameters in Table II, where we specify the values of the decoupling temperature, $\Delta N_{\rm eff}$, $\Omega_a h^2$, and $k_{\rm fs}$ for the range of axion masses considered here, (0.1,3) eV.

TABLE II. Values for the axion parameters, T_D, $\Delta N_{\rm eff}$, $\Omega_a h^2$ and $k_{\rm fs}$ for the lower and upper prior choice of m_a explored here.

Axion parameter		
m_a (eV)	0.1	3
T_D (MeV)	245.6	43.2
$\Omega_a h^2$	0.0003	0.016
$\Delta N_{\rm eff}$	0.18	0.43
$k_{\rm fs}$ (h/Mpc)	0.06	1.46

C. Cosmological measurements

Our baseline data set consists of CMB measurements. These include the temperature data from the Planck satellite, (see Refs. [28,38]) together with the WMAP 9-year polarization measurements, following [39]. We also consider high multipole data from the South Pole Telescope [40] as well as from the Atacama Cosmology Telescope [41]. The combination of all the above CMB data is referred to as the CMB data set.

Galaxy clusters represent an independent tool to probe the cosmological parameters. Cluster surveys usually report their measurements by means of the so-called cluster normalization condition, $\sigma_8 \Omega_m^\gamma$, where $\gamma \sim 0.4$ [42–44]. We shall use here the cluster normalization condition as measured by the Planck Sunyaev-Zeldovich (PSZ) 2013 catalog [45], referring to it as the PSZ data set. The PSZ measurements of the cluster mass function provide the constraint $\sigma_8(\Omega_m/0.27)^{0.3} = 0.764 \pm 0.025$. As there exists a strong degeneracy between the value of the σ_8 parameter and the cluster mass bias, it is possible to fix the value of the bias parameter according to the results arising from numerical simulations. In this last case, the error on the cluster normalization condition from the PSZ catalog is considerably reduced: $\sigma_8(\Omega_m/0.27)^{0.3} = 0.78 \pm 0.01$. In our analyses, we shall consider the two PSZ measurements of the cluster normalization condition to illustrate the impact of the cluster mass bias in the thermal axion mass bounds, as recently explored in Ref. [46] for the neutrino mass case. Figure 2 illustrates the prediction for the cluster normalisation condition, $\sigma_8(\Omega_m/0.27)^{0.3}$, as a function of the thermal axion mass. We also show the current PSZ measurements with their associated 95% C.L. uncertainties, including those in which the cluster mass bias parameter is fixed. Notice that the normalization condition decreases as the axion mass increases due to the decrease induced in the σ_8 parameter in the presence of axion masses: the larger the axion mass, the larger the reduction in the matter power spectra will be.

Tomographic weak lensing surveys are sensitive to the overall amplitude of the matter power spectrum by measuring the correlations in the observed shape of distant galaxies induced by the intervening large-scale structure. The matter power spectrum amplitude depends on both the σ_8 clustering parameter and the matter density Ω_m.

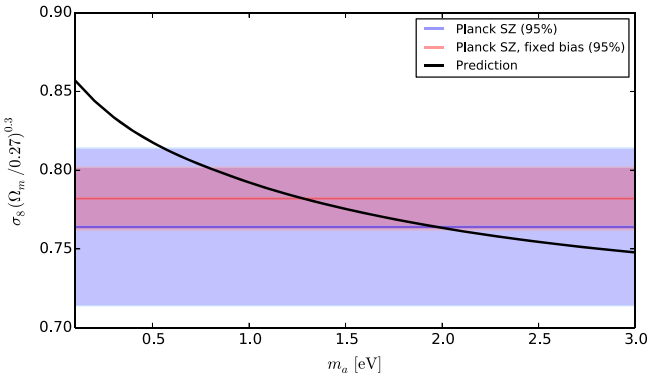

FIG. 2 (color online). Cluster normalisation condition, $\sigma_8(\Omega_m/0.27)^{0.3}$, as a function of the thermal axion mass. We also show the current PSZ measurements with their associated 95% C.L. uncertainties.

Consequently, tomographic lensing surveys, via measurements of the galaxy power shear spectra, provide additional and independent constraints in the (σ_8, Ω_m) plane. The Canada-France-Hawaii Telescope Lensing Survey, CFHTLenS, with six tomographic redshift bins (from $z = 0.28$ to $z = 1.12$) provides a constraint on the relationship between σ_8 and Ω_m of $\sigma_8(\Omega_m/0.27)^{0.46} = 0.774 \pm 0.040$ [47]. We shall refer to this data set as CFHT.

We also address here the impact of a Gaussian prior on the Hubble constant $H_0 = 70.6 \pm 3.3$ km/s/Mpc from an independent reanalysis of Cepheid data [48], referring to this prior as the HST data set.

We have also included measurements of the large-scale structure of the Universe in their geometrical form, i.e., in the form of baryon acoustic oscillations (BAO). Although previous studies in the literature have shown that, for constraining hot thermal relics, the shape information contained in the galaxy power spectrum is more powerful when dealing simultaneously with extra relativistic species and hot thermal relic masses [49,50], we exploit here the BAO signature, as the contribution from the thermal axions to the relativistic number of species is not very large (see Table II), and current measurements from galaxy surveys are mostly reported in the geometrical (BAO) form.

The BAO wiggles, imprinted in the power spectrum of the galaxy distribution, result from the competition in the coupled photon-baryon fluid between radiation pressure and gravity. The BAO measurements that have been considered in our numerical analyses include the results from the WiggleZ [51], the 6dF [52], and the SDSS II surveys [53,54], at redshifts of $z = 0.44, 0.6, 0.73$, $z = 0.106$, and $z = 0.35$, respectively. We also include in our analyses as well the Data Release 11 (DR11) BAO signal of the BOSS experiment [55], which provides the most precise distant constraints [56] measuring both the Hubble parameter and the angular diameter distance at an effective redshift of 0.57. Figure 3 illustrates the spherically averaged BAO distance, $D_V(z) \propto D_A^2(z)/H(z)$, as a function of the axion mass, at a redshift of $z = 0.57$, as well as the measurement from the BOSS experiment with 95% C.L. error bars [56]. Notice that, from background measurements only, there exists a strong degeneracy between the cold dark matter mass-energy density and the axion one. The solid black line in Fig. 3 shows the spherically averaged BAO distance if all the cosmological parameters are fixed, including ω_c. The spherically averaged BAO distance deviates strongly from the ΛCDM prediction. However, if ω_c is varied while m_a is changed (in order to keep the total matter mass-energy density constant, see the dotted blue line in Fig. 3), the spherically averaged BAO distance approaches to its expected value in a ΛCDM cosmology.

D. Compatibility of data

It has been pointed out (see Sec. 5.5 of Ref. [27] and also Refs. [10,57]) that the value of σ_8 reported by cluster measurements and the value estimated from Planck CMB measurements show a tension at the $\sim 2\sigma$ level. These discrepancies may arise due to the lack of a full understanding of the cluster mass calibrations. Although some studies in the literature, including the present one, show that in extended cosmological models with nonzero neutrino masses the discrepancies previously mentioned could be alleviated, the results from Ref. [57] show, using also Bayesian evidence, that a canonical ΛCDM scenario with no massive neutrinos is preferred over its neutrino extensions by several combinations of cosmological data sets. Therefore, the results presented here and obtained when considering cluster data depend strongly on the reliability of low-redshift cluster data. If future data confirm current low-redshift cluster measurements, one could further test

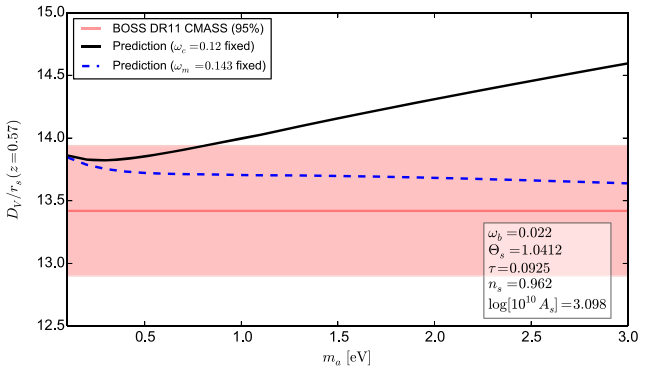

FIG. 3 (color online). The solid black line depicts the spherically averaged BAO distance $D_V(z)$, as a function of the axion mass, at a redshift of $z = 0.57$, after keeping fixed all the remaining cosmological parameters, the cold dark matter included. The dashed blue line depicts the equivalent but keeping fixed the total matter mass-energy density (and consequently changing the cold dark matter ω_c). The bands show the measurement from the BOSS experiment (DR11) with its associated 95% C.L. error.

TABLE III. The 95% C.L. constraints on the physical cold dark matter density $\Omega_c h^2$, the axion mass m_a (in eV), the clustering parameter σ_8, the relative matter energy density Ω_m, and the $P_{s,j}$ parameters for the PPS nodes from the different combinations of data sets explored here in the $\Lambda\mathrm{CDM} + m_a$ model, considering the PCHIP PPS modeling.

	CMB	CMB + HST	CMB + BAO	CMB + BAO +HST	CMB + BAO HST + CFHT	CMB + BAO + HST +PSZ (fixed bias)	CMB + BAO +HST + PSZ
$\Omega_c h^2$	$0.127^{+0.007}_{-0.007}$	$0.122^{+0.006}_{-0.006}$	$0.122^{+0.003}_{-0.003}$	$0.121^{+0.003}_{-0.003}$	$0.120^{+0.003}_{-0.003}$	$0.118^{+0.002}_{-0.002}$	$0.119^{+0.003}_{-0.004}$
m_a [eV]	Unconstrained	< 1.31	< 0.89	< 0.91	< 1.29	$1.00^{+0.50}_{-0.48}$	$0.93^{+0.70}_{-0.71}$
σ_8	$0.788^{+0.079}_{-0.086}$	$0.821^{+0.052}_{-0.074}$	$0.827^{+0.044}_{-0.057}$	$0.825^{+0.045}_{-0.059}$	$0.793^{+0.049}_{-0.058}$	$0.760^{+0.023}_{-0.022}$	$0.767^{+0.046}_{-0.044}$
Ω_m	$0.369^{+0.070}_{-0.065}$	$0.314^{+0.045}_{-0.039}$	$0.308^{+0.016}_{-0.015}$	$0.304^{+0.016}_{-0.014}$	$0.302^{+0.016}_{-0.015}$	$0.304^{+0.016}_{-0.015}$	$0.304^{+0.016}_{-0.016}$
$P_{s,1}$	< 8.13	< 8.17	< 7.91	< 8.06	< 7.85	< 8.09	< 8.11
$P_{s,2}$	$1.09^{+0.42}_{-0.35}$	$1.01^{+0.43}_{-0.35}$	$1.01^{+0.40}_{-0.32}$	$0.99^{+0.42}_{-0.33}$	$1.02^{+0.43}_{-0.34}$	$1.01^{+0.42}_{-0.33}$	$1.05^{+0.43}_{-0.38}$
$P_{s,3}$	$0.68^{+0.39}_{-0.36}$	$0.71^{+0.39}_{-0.39}$	$0.71^{+0.39}_{-0.37}$	$0.72^{+0.39}_{-0.38}$	$0.69^{+0.39}_{-0.37}$	$0.70^{+0.40}_{-0.38}$	$0.69^{+0.40}_{-0.39}$
$P_{s,4}$	$1.14^{+0.24}_{-0.22}$	$1.15^{+0.24}_{-0.22}$	$1.15^{+0.23}_{-0.21}$	$1.15^{+0.23}_{-0.20}$	$1.15^{+0.23}_{-0.21}$	$1.15^{+0.23}_{-0.21}$	$1.15^{+0.22}_{-0.21}$
$P_{s,5}$	$1.02^{+0.11}_{-0.10}$	$1.01^{+0.11}_{-0.11}$	$1.00^{+0.11}_{-0.10}$	$1.00^{+0.11}_{-0.10}$	$0.99^{+0.11}_{-0.10}$	$0.99^{+0.11}_{-0.10}$	$0.99^{+0.11}_{-0.11}$
$P_{s,6}$	$1.03^{+0.08}_{-0.07}$	$1.00^{+0.08}_{-0.07}$	$1.00^{+0.08}_{-0.07}$	$1.00^{+0.08}_{-0.07}$	$0.98^{+0.07}_{-0.06}$	$0.98^{+0.07}_{-0.07}$	$0.98^{+0.08}_{-0.07}$
$P_{s,7}$	$0.99^{+0.07}_{-0.06}$	$0.98^{+0.08}_{-0.07}$	$0.98^{+0.07}_{-0.07}$	$0.98^{+0.08}_{-0.07}$	$0.96^{+0.07}_{-0.06}$	$0.95^{+0.07}_{-0.06}$	$0.96^{+0.07}_{-0.06}$
$P_{s,8}$	$0.94^{+0.06}_{-0.06}$	$0.95^{+0.08}_{-0.07}$	$0.95^{+0.07}_{-0.06}$	$0.95^{+0.08}_{-0.07}$	$0.94^{+0.07}_{-0.06}$	$0.94^{+0.07}_{-0.06}$	$0.94^{+0.07}_{-0.06}$
$P_{s,9}$	$0.92^{+0.06}_{-0.05}$	$0.94^{+0.08}_{-0.06}$	$0.94^{+0.07}_{-0.06}$	$0.94^{+0.08}_{-0.06}$	$0.93^{+0.07}_{-0.06}$	$0.93^{+0.07}_{-0.06}$	$0.94^{+0.07}_{-0.06}$
$P_{s,10}$	$0.90^{+0.06}_{-0.06}$	$0.91^{+0.08}_{-0.07}$	$0.91^{+0.07}_{-0.06}$	$0.91^{+0.08}_{-0.06}$	$0.90^{+0.07}_{-0.06}$	$0.90^{+0.07}_{-0.06}$	$0.90^{+0.07}_{-0.07}$
$P_{s,11}$	$1.25^{+0.30}_{-0.28}$	$1.24^{+0.32}_{-0.31}$	$1.23^{+0.31}_{-0.31}$	$1.24^{+0.31}_{-0.31}$	$1.22^{+0.30}_{-0.31}$	$1.22^{+0.32}_{-0.28}$	$1.23^{+0.31}_{-0.30}$
$P_{s,12}$	Unconstrained	Unconstrained	Unconstrained	Unconstrained	Unconstrained	Unconstrained	Unconstrained

some of the possible beyond the ΛCDM models using particle physics experiments. For instance, the existence of a full thermal sterile neutrino could be tested with neutrino oscillation experiments, and the active neutrino mass could also be tested by tritium experiments or, if the neutrino is a Majorana particle, by neutrinoless double beta decay searches.

III. RESULTS

Table III depicts our results in the first scenario explored here, in which the axion mass is a free parameter and the PPS is described by the approach specified in Sec. II A. Concerning CMB measurements only, the bounds on the thermal axion masses are largely relaxed in the case in which the PPS is not described by a simple power law, as can be noticed after comparing the results depicted in Table III with those shown in Table IV. This can be understood in terms of Fig. 4, which illustrates the degeneracies in the temperature anisotropies between the thermal axion mass and the PCHIP PPS. Figure 4 shows the temperature anisotropies for a ΛCDM model and a power-law PPS (solid red line), for a 2 eV thermal axion mass and a power-law PPS (dashed blue line), and for a ΛCDM model with the PPS described by the PCHIP model explored here (dotted black line), with values for the $P_{s,j}$ chosen to match the nonzero thermal axion mass curve, according to their current allowed regions (see Table III). More concretely, we have used the following values for the PPS parameters: $P_{s,1} = 1.15$, $P_{s,2} = 1.073$, $P_{s,3} = 1.058$, $P_{s,4} = 1.03$, $P_{s,5} = 0.99$, $P_{s,6} = 0.97$, $P_{s,7} = 0.966$, $P_{s,8} = 0.932$, $P_{s,9} = 0.91$, $P_{s,10} = 0.86$, $P_{s,11} = 0.84$, and $P_{s,12} = 0.77$. Notice that the case of a 2 eV thermal axion can be easily mimicked by a simple ΛCDM model if the assumptions concerning the PPS shape are relaxed. We also add in this figure the measurements of the photon temperature anisotropies from the Planck 2013 data release [27].

The addition to the CMB data of the HST prior on the Hubble constant provides a 95% C.L. upper limit on the thermal axion mass of 1.31 eV,[1] while the further addition of the BAO measurements brings this constraint down to 0.91 eV, as these last data sets are directly sensitive to the free-streaming nature of the thermal axion. Notice that these two 95% C.L. upper bounds are very similar to the ones obtained when considering the standard power-law power spectrum, which are 1.56 eV and 0.83 eV for the CMB + HST and CMB + HST + BAO data combinations, respectively.

Interestingly, when adding the CFHT bounds on the $\sigma_8 - \Omega_m$ relationship, the bounds on the thermal axion mass become weaker. The reason for that is due to the lower σ_8 values preferred by weak lensing measurements, values that can be achieved by allowing for higher axion masses. The larger the axion mass, the larger is the reduction of the matter power spectrum at small (i.e. cluster) scales,

[1]There exists a very large degeneracy between H_0 and the neutrino masses when restricting the numerical analyses to CMB measurements. The addition of the HST prior on the Hubble constant helps enormously in breaking this degeneracy, see [50].

TABLE IV. 95% C.L. constraints on $\Omega_c h^2$, the axion mass m_a (in eV), σ_8, Ω_m, $\log(10^{10}A_s)$ and n_s from the different combinations of data sets explored here in the ΛCDM + m_a model, assuming the standard power-law PPS.

	CMB	CMB + HST	CMB + BAO	CMB + BAO +HST	CMB + BAO +HST + CFHT	CMB + BAO + HST +PSZ (fixed bias)	CMB + BAO +HST + PSZ
$\Omega_c h^2$	$0.124^{+0.006}_{-0.005}$	$0.124^{+0.005}_{-0.005}$	$0.122^{+0.004}_{-0.004}$	$0.121^{+0.004}_{-0.004}$	$0.120^{+0.003}_{-0.003}$	$0.119^{+0.003}_{-0.003}$	$0.120^{+0.003}_{-0.003}$
m_a [eV]	< 1.83	< 1.56	< 0.84	< 0.83	< 1.16	$0.80^{+0.53}_{-0.50}$	< 1.26
σ_8	$0.785^{+0.064}_{-0.083}$	$0.791^{+0.057}_{-0.076}$	$0.803^{+0.041}_{-0.048}$	$0.803^{+0.041}_{-0.048}$	$0.783^{+0.047}_{-0.054}$	$0.758^{+0.028}_{-0.029}$	$0.767^{+0.045}_{-0.045}$
Ω_m	$0.337^{+0.048}_{-0.044}$	$0.328^{+0.041}_{-0.039}$	$0.310^{+0.025}_{-0.023}$	$0.308^{+0.024}_{-0.023}$	$0.305^{+0.025}_{-0.024}$	$0.307^{+0.027}_{-0.026}$	$0.306^{+0.027}_{-0.025}$
$\log[10^{10}A_s]$	$3.10^{+0.05}_{-0.05}$	$3.10^{+0.05}_{-0.05}$	$3.10^{+0.05}_{-0.05}$	$3.10^{+0.05}_{-0.05}$	$3.10^{+0.05}_{-0.05}$	$3.09^{+0.05}_{-0.05}$	$3.09^{+0.05}_{-0.05}$
n_s	$0.961^{+0.014}_{-0.015}$	$0.963^{+0.013}_{-0.014}$	$0.968^{+0.011}_{-0.011}$	$0.969^{+0.011}_{-0.011}$	$0.971^{+0.011}_{-0.011}$	$0.973^{+0.011}_{-0.011}$	$0.972^{+0.011}_{-0.011}$

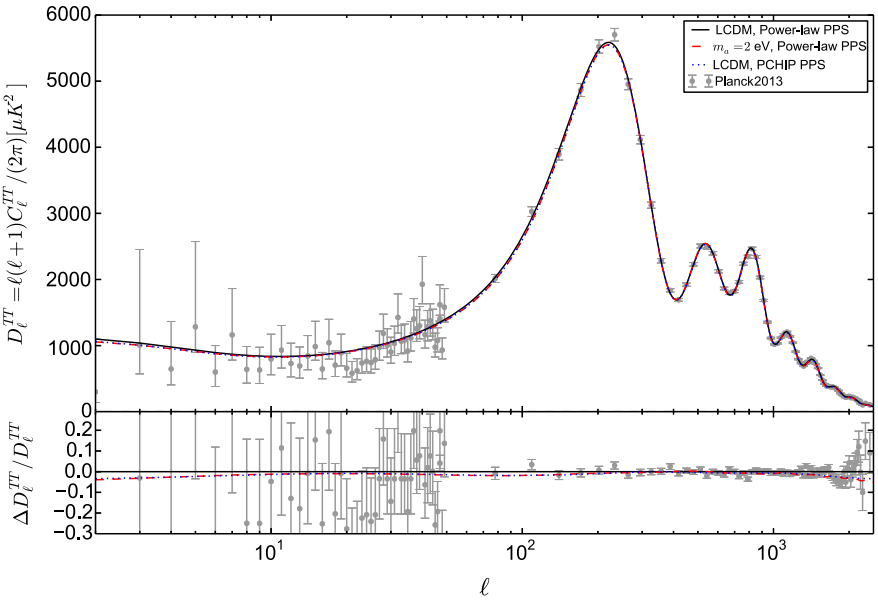

FIG. 4 (color online). Temperature anisotropies for the pure ΛCDM model and a power-law PPS (solid red line), for a 2 eV thermal axion mass and a power-law PPS (dashed blue line) and for the standard ΛCDM model but the PPS described by the PCHIP model (dotted black line). The data points and the error bars in the left panel show the measurements of the photon temperature anisotropies arising from the Planck 2013 data release [27].

leading consequently to a smaller value of the clustering parameter σ_8.

If we instead consider now the PSZ data set with fixed cluster mass bias, together with the CMB, BAO and HST measurements, a nonzero value of the thermal axion mass of $\sim$1 eV ($\sim$0.80 eV) is favored at $\sim 4\sigma$ ($\sim 3\sigma$) level, when considering the PCHIP (standard power-law) PPS approach.[2] However, these results must be regarded as an illustration of what could be achieved with future cluster mass calibrations, as the Planck collaboration has recently shown in their analyses of the 2015 Planck cluster catalog [46]. When more realistic approaches for the cluster mass bias are used, the errors on the so-called cluster normalization condition are larger, and, consequently, the preference for a nonzero axion mass of 1 eV is only mild in the PCHIP PPS case, while in the case of a standard power-law PPS such an evidence completely disappears.

Figure 5 (left panel) shows the 68% and 95% C.L. allowed regions in the (m_a, $\Omega_c h^2$) plane for some of the possible data combinations explored in this study, and assuming the PCHIP PPS modeling. Notice that, when adding BAO measurements, lower values of the physical cold dark matter density are preferred. This is due to the fact that large-scale structure allows for lower axion masses than CMB data alone. The lower is the thermal axion mass, the lower is the amount of hot dark matter and consequently the lower should be the cold dark matter component. This effect is clear from the results shown in Table III and Table IV, where the values of the physical cold dark matter density $\Omega_c h^2$ and of the relative current matter density Ω_m arising from our numerical fits are shown, for the different data combinations considered here.

[2]A similar effect when considering PSZ data for constraining either thermal axion or neutrino masses has also been found in Refs. [10,58–61].

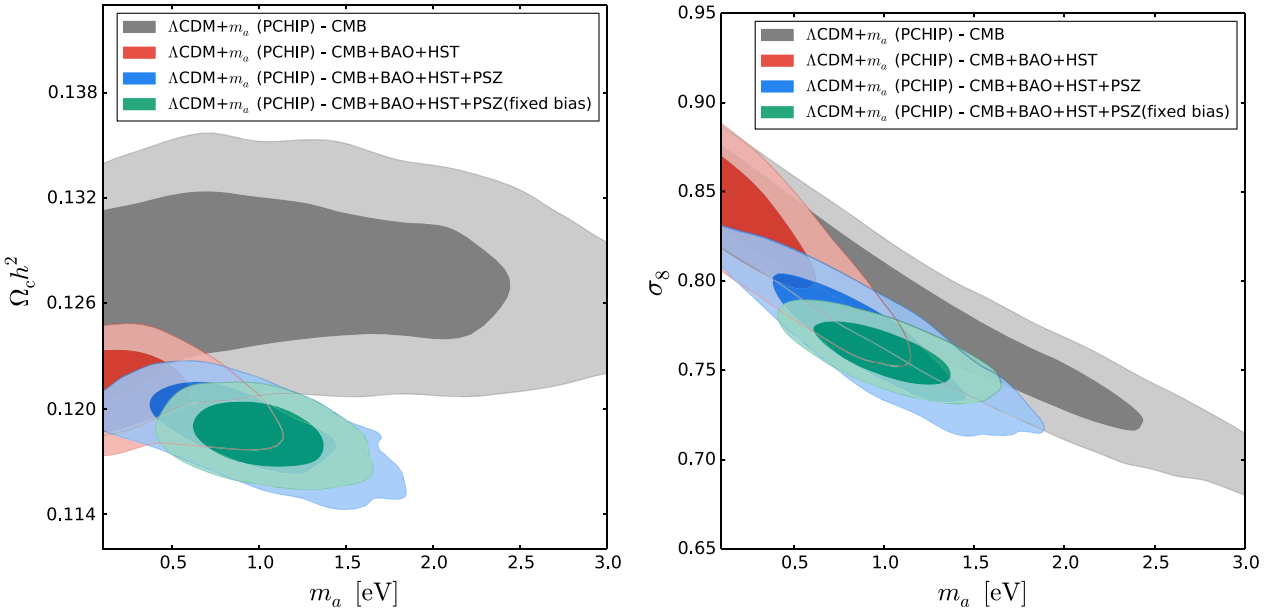

FIG. 5 (color online). The left panel depicts the 68% and 95% C.L. allowed regions in the $(m_a, \Omega_c h^2)$ plane for different possible data combinations, when a PCHIP PPS is assumed. The right panel shows the equivalent but in the (m_a, σ_8) plane.

The right panel of Fig. 5 shows the 68% and 95% C.L. allowed regions in the (m_a, σ_8) plane in the PCHIP PPS scenario. The lower values of the σ_8 clustering parameter preferred by PSZ data (see the results shown in Table III and Table IV) are translated into a preference for nonzero thermal axion masses. Larger values of m_a will enhance the matter power spectrum suppression at scales below the axion free-streaming scale, leading to smaller values of the σ_8 clustering parameter, as preferred by PSZ measurements. The evidence for nonzero axion masses is more significant when fixing the cluster mass bias in the PSZ data analyses.

Figure 6 shows the equivalent to Fig. 5 but for a standard power-law PPS. Notice that, except for the case in which CMB measurements are considered alone, the thermal axion mass constraints do not change significantly, if they are compared to the PCHIP PPS modeling. This fact clearly states the robustness of the cosmological bounds on

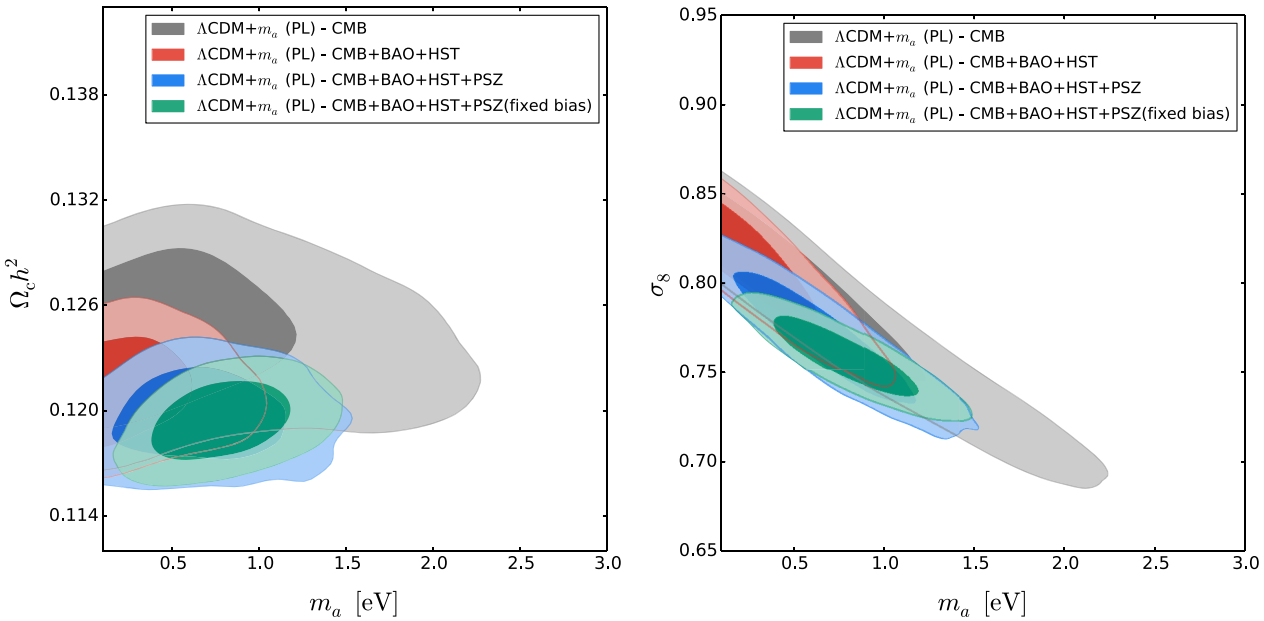

FIG. 6 (color online). The left panel depicts the 68% and 95% C.L. allowed regions in the $(m_a, \Omega_c h^2)$ plane for different possible data combinations, when a power-law PPS is assumed. The right panel shows the equivalent but in the (m_a, σ_8) plane.

TABLE V. The 95% C.L. constraints on the physical cold dark matter density $\Omega_c h^2$, the axion mass m_a, the sum of the active neutrino masses $\sum m_\nu$ (both in eV), the clustering parameter σ_8, the relative matter energy density Ω_m and the $P_{s,j}$ parameters for the PPS nodes from the different combinations of data sets explored here in the $\Lambda\mathrm{CDM} + m_a + \sum m_\nu$ model, considering the PCHIP PPS modeling.

	CMB	CMB + HST	CMB + BAO	CMB + BAO +HST	CMB + BAO +HST + CFHT	CMB + BAO + HST +PSZ (fixed bias)	CMB + BAO +HST + PSZ
$\Omega_c h^2$	$0.130^{+0.008}_{-0.007}$	$0.125^{+0.006}_{-0.007}$	$0.121^{+0.003}_{-0.003}$	$0.121^{+0.003}_{-0.003}$	$0.119^{+0.003}_{-0.003}$	$0.118^{+0.003}_{-0.003}$	$0.118^{+0.003}_{-0.003}$
m_a [eV]	< 2.48	< 1.64	< 0.81	< 0.86	< 1.23	$0.81^{+0.59}_{-0.69}$	< 1.46
$\sum m_\nu$ [eV]	< 2.11	< 0.43	< 0.22	< 0.21	< 0.27	< 0.32	< 0.35
σ_8	$0.700^{+0.172}_{-0.202}$	$0.803^{+0.082}_{-0.091}$	$0.833^{+0.055}_{-0.058}$	$0.834^{+0.058}_{-0.064}$	$0.787^{+0.052}_{-0.055}$	$0.766^{+0.043}_{-0.044}$	$0.757^{+0.023}_{-0.022}$
Ω_m	$0.486^{+0.277}_{-0.193}$	$0.356^{+0.064}_{-0.062}$	$0.309^{+0.016}_{-0.015}$	$0.308^{+0.016}_{-0.015}$	$0.306^{+0.015}_{-0.015}$	$0.308^{+0.016}_{-0.016}$	$0.308^{+0.017}_{-0.016}$
$P_{s,1}$	< 8.01	< 8.13	< 7.00	< 8.17	< 7.59	< 8.29	< 8.18
$P_{s,2}$	$1.17^{+0.42}_{-0.38}$	$1.09^{+0.41}_{-0.37}$	$1.03^{+0.40}_{-0.35}$	$1.02^{+0.39}_{-0.34}$	$1.02^{+0.40}_{-0.32}$	$1.03^{+0.36}_{-0.34}$	$1.05^{+0.40}_{-0.36}$
$P_{s,3}$	$0.66^{+0.37}_{-0.35}$	$0.69^{+0.38}_{-0.37}$	$0.70^{+0.38}_{-0.38}$	$0.72^{+0.38}_{-0.37}$	$0.68^{+0.37}_{-0.33}$	$0.71^{+0.40}_{-0.39}$	$0.69^{+0.39}_{-0.37}$
$P_{s,4}$	$1.17^{+0.23}_{-0.23}$	$1.15^{+0.23}_{-0.22}$	$1.15^{+0.22}_{-0.21}$	$1.15^{+0.21}_{-0.21}$	$1.15^{+0.20}_{-0.19}$	$1.14^{+0.21}_{-0.20}$	$1.16^{+0.22}_{-0.21}$
$P_{s,5}$	$1.05^{+0.15}_{-0.14}$	$1.01^{+0.11}_{-0.10}$	$1.00^{+0.11}_{-0.10}$	$1.00^{+0.11}_{-0.10}$	$0.98^{+0.11}_{-0.10}$	$0.99^{+0.11}_{-0.10}$	$0.98^{+0.11}_{-0.10}$
$P_{s,6}$	$1.04^{+0.09}_{-0.08}$	$1.01^{+0.08}_{-0.07}$	$1.00^{+0.07}_{-0.07}$	$1.00^{+0.07}_{-0.07}$	$0.98^{+0.07}_{-0.06}$	$0.98^{+0.07}_{-0.07}$	$0.98^{+0.07}_{-0.07}$
$P_{s,7}$	$0.99^{+0.06}_{-0.06}$	$0.98^{+0.07}_{-0.06}$	$0.98^{+0.07}_{-0.07}$	$0.98^{+0.07}_{-0.07}$	$0.95^{+0.07}_{-0.06}$	$0.95^{+0.06}_{-0.06}$	$0.95^{+0.07}_{-0.06}$
$P_{s,8}$	$0.93^{+0.06}_{-0.05}$	$0.94^{+0.06}_{-0.06}$	$0.95^{+0.07}_{-0.07}$	$0.95^{+0.07}_{-0.07}$	$0.93^{+0.07}_{-0.05}$	$0.94^{+0.07}_{-0.06}$	$0.93^{+0.07}_{-0.06}$
$P_{s,9}$	$0.91^{+0.06}_{-0.05}$	$0.93^{+0.06}_{-0.06}$	$0.94^{+0.07}_{-0.06}$	$0.94^{+0.07}_{-0.06}$	$0.93^{+0.07}_{-0.06}$	$0.93^{+0.06}_{-0.06}$	$0.93^{+0.07}_{-0.06}$
$P_{s,10}$	$0.90^{+0.06}_{-0.06}$	$0.90^{+0.07}_{-0.06}$	$0.91^{+0.07}_{-0.07}$	$0.91^{+0.08}_{-0.07}$	$0.88^{+0.07}_{-0.06}$	$0.89^{+0.07}_{-0.07}$	$0.90^{+0.07}_{-0.07}$
$P_{s,11}$	$2.18^{+0.85}_{-0.77}$	$2.07^{+0.81}_{-0.80}$	$2.12^{+0.90}_{-0.86}$	$2.15^{+0.95}_{-0.94}$	$1.64^{+0.79}_{-0.75}$	$1.83^{+0.87}_{-0.86}$	$1.84^{+0.86}_{-0.87}$
$P_{s,12}$	Unconstrained	Unconstrained	Unconstrained	Unconstrained	Unconstrained	Unconstrained	Unconstrained

thermal axion masses and it is applicable to the remaining cosmological parameters, see Tables III and IV. Note that, for the standard case of a power-law PPS, the preference for nonzero axion masses appears only when considering the (unrealistic) PSZ analysis with a fixed cluster mass bias. When more realistic PSZ measurements of the cluster normalization condition are exploited, there is no preference for a nonzero thermal axion mass.

The last scenario we explore here is a $\Lambda\mathrm{CDM} + m_a + \sum m_\nu$ universe, in which we consider two coexisting hot dark matter species: thermal axions and three active (massive) neutrinos. Table V illustrates the equivalent of Table III but including the active neutrino masses in the MCMC parameters. We do not perform here the analysis for the hot mixed dark matter model with the standard power-law matter power spectrum, as it was already presented previously in Ref. [10]. If we compare to the standard power-law case, we find that the bounds on the axion and neutrino masses presented here are very similar. Furthermore, no evidence for neutrino masses nor for a nonzero axion mass appears in this mixed hot dark matter scenario (except for the axion case and only if considering PSZ clusters with the bias fixed). The reason for that is due to the strong degeneracy between m_a and $\sum m_\nu$, see Fig. 7, where one can notice that these two parameters are negatively correlated: an increase in the axion mass will increase the amount of the hot dark matter component. In order to compensate the changes in both the CMB temperature anisotropies (via the early ISW effect) and in the power spectrum (via the suppression at small scales of galaxy clustering), the contribution to the hot dark matter from the neutrinos should be reduced. We have shown in Fig. 7 three possible data combinations. Notice that for the case in which PSZ cluster measurements (with the bias fixed) are included the strong degeneracy between m_a and

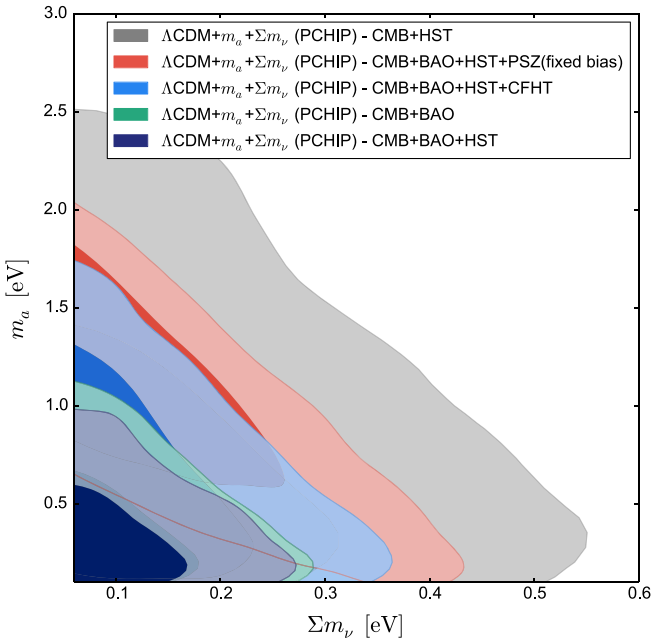

FIG. 7 (color online). The 68% and 95% C.L. allowed regions in the ($\sum m_\nu$, m_a) plane, both in eV, for three different possible data combinations, when a PCHIP PPS is assumed.

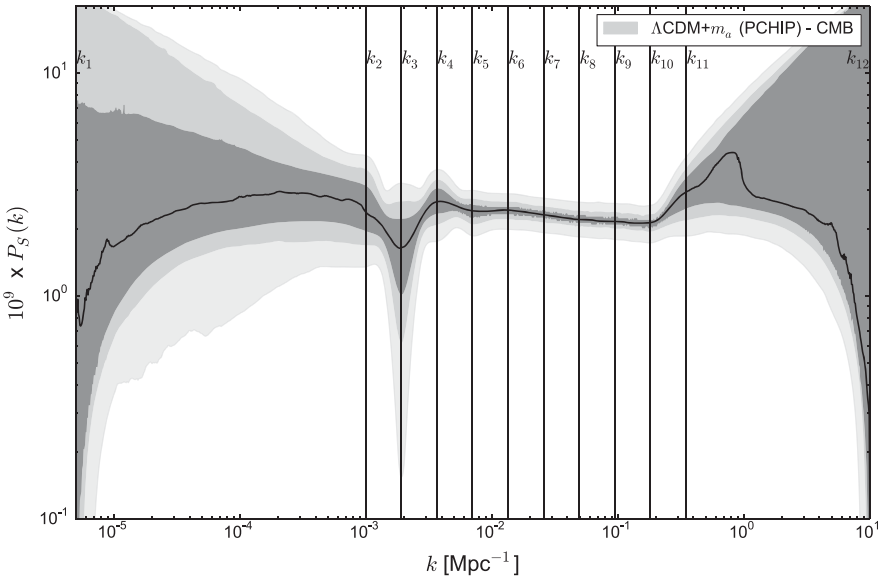

FIG. 8. The 68%, 95%, and 99% C.L. allowed regions for the PCHIP PPS scale dependence in the $\Lambda\mathrm{CDM} + m_a$ model, using CMB data only. The bands are obtained with a marginalization of the posterior distribution for each different value of the wave number k in a fine grid. The black line represents the peak of the posterior distribution at each value of k.

$\sum m_\nu$ is partially broken, due to the smaller value of σ_8 preferred by the former data set. However, these results strongly rely on the numerical results concerning the cluster mass bias and therefore the evidence for $m_a \neq 0$ should be regarded as what could be obtained in if these measurements are further supported by independent data from future cluster surveys.

Besides the results concerning the thermal axion mass and the standard ΛCDM parameters, we also obtain constraints on the form of the PPS when modeled according to the PCHIP scenario. The 95% C.L. limits for the $P_{s,j}$ parameters are shown in Table III, while an example of the reconstructed PPS is given in Fig. 8, where we show the 68%, 95%, and 99% C.L. allowed regions arising from a fit to CMB data of the PCHIP PPS scale dependence, in the context of a $\Lambda\mathrm{CDM} + m_a$ model. We do not show the corresponding figures obtained from all the other data combinations since they are equivalent to Fig. 8, as one can infer from the very small differences in the 95% C.L. allowed ranges for the $P_{s,j}$ parameters arising from different data sets; see Table III. Note that both $P_{s,1}$ and $P_{s,12}$ are poorly constrained at this confidence level: the reason for that is the absence of measurements at their corresponding wave numbers. All the remaining $P_{s,j}$, with $j = 2, \ldots, 11$ are well constrained. In particular, in the range between k_5 and k_{10} [see Eq. (3)], the $P_{s,j}$ are determined within a few percent accuracy. Indeed, in the range covered between these nodes, the PPS does not present features and can be perfectly described by a power-law parametrization. Among the interesting features outside the former range, we can notice in Fig. 8 a significant dip at wave numbers around $k = 0.002$ Mpc^{-1}, which comes from the dip at $\ell = 20$–30 in the CMB temperature power spectrum and a small bump around $k = 0.0035$ Mpc^{-1}, corresponding to the increase at $\ell \simeq 40$. These features have been obtained in previous works [11,24,25] using different methods and data sets. In addition, we obtain an increase of power at $k \simeq 0.2$ Mpc^{-1}, necessary to compensate for the effects of the thermal axion mass in both the temperature anisotropies and the large-scale structure of the Universe.

IV. CONCLUSIONS

Axions provide the most elegant scenario to solve the strong *CP* problem and may be produced in the early Universe via both thermal and nonthermal processes. While nonthermal axions are highly promising cold dark matter candidates, their thermal companions will contribute to the hot dark matter component of the Universe, together with the (light) three active neutrinos of the standard model of elementary particles. Therefore, the cosmological consequences of light massive thermal axions are very much like those associated with neutrinos, as axions also have a free-streaming nature, suppressing structure formation at small scales. Furthermore, these light thermal axions will also contribute to the dark radiation background, leading to deviations of the relativistic degrees of freedom N_{eff} from its canonically expected value of $N_{\mathrm{eff}} = 3.046$. Based on these signatures, several studies have been carried out in the literature deriving bounds on the thermal axion mass [5–10].

Nevertheless, these previous constraints assumed that the underlying primordial perturbation power spectrum follows the usual power-law description governed, in its most economical form, by an amplitude and a scalar spectral

index. Here we have relaxed such an assumption, in order to test the robustness of the cosmological axion mass bounds. Using an alternative, nonparametric description of the primordial power spectrum of the scalar perturbations, named PCHIP and introduced in Ref. [11], we have shown that, in practice, when combining CMB measurements with low redshift cosmological probes, the axion mass constraints are only mildly sensitive to the primordial power spectrum choice and, therefore, are not strongly dependent on the particular details of the underlying inflationary model. These results agree with the findings of Ref. [29] for the neutrino mass case. The tightest bound we find in the PCHIP primordial power spectrum approach is obtained when considering BAO measurements together with CMB data, with $m_a < 0.89$ eV at 95% C.L. In the standard power-law primordial power spectrum modeling, the tightest bound is $m_a < 0.83$ eV at 95% C.L., obtained when combining BAO, CMB, and HST measurements. Notice that these bounds are very similar, confirming the robustness of the cosmological axion mass measurements versus the primordial power spectrum modeling.

Interestingly, both weak lensing measurements and cluster number counts weaken the thermal axion mass bounds. The reason for that is due to the lower σ_8 values preferred by these measurements, which could be generated by a larger axion mass. More concretely, Planck cluster measurements provide a measurement of the so-called cluster normalization condition, which establishes a relationship between the clustering parameter σ_8 and the current matter mass-energy density Ω_m. However, the errors on this relationship depend crucially on the knowledge of the cluster mass bias. A conservative approach for the cluster mass calibration results in mild (zero) evidence for a nonzero axion mass of 1 eV in the PCHIP (power-law) PPS case. We also illustrate a case in which the cluster mass bias is fixed, to forecast the expected results from future cosmological measurements. In this case, a nonzero value of the thermal axion mass of $\sim$1 eV ($\sim$0.80 eV) is favored at $\sim 4\sigma$ ($\sim 3\sigma$) level, when considering the PCHIP (power-law) PPS approach. When considering additional hot relics in our analyses, as the sum of the three active neutrino masses, the evidence for a $\sim$1 eV thermal axion mass disappears almost completely. Furthermore, these values of axion masses correspond to an axion coupling constant $f_a = 6 \times 10^6$ GeV, which seems to be in tension with the limits extracted from the neutrino signal duration from SN 1987A [62,63] (albeit these limits depend strongly on the precise axion emission rate and still remain rough estimates). Precise cluster mass calibration measurements are, therefore, mandatory to assess whether there exists a cosmological indication for nonzero axion masses, as the cluster mass bias is highly correlated with the clustering parameter σ_8, which, in turn, is highly affected by the free-streaming nature of a hot dark matter component, as thermal axions.

ACKNOWLEDGMENTS

O. M. is supported by PROMETEO II/2014/050, by the Spanish Grant No. FPA2011–29678 of the MINECO and by PITN-GA-2011-289442-INVISIBLES. This work has been done within the Labex ILP (reference ANR-10-LABX-63) part of the Idex SUPER and received financial state aid managed by the Agence Nationale de la Recherche, as part of the program Investissements d'avenir under the reference ANR-11-IDEX-0004-02. E. D. V. acknowledges the support of the European Research Council via Grant No. 267117 (DARK, P.I. Joseph Silk).

[1] R. D. Peccei and H. R. Quinn, Phys. Rev. Lett. **38**, 1440 (1977); Phys. Rev. D **16**, 1791 (1977).
[2] S. Weinberg, Phys. Rev. Lett. **40**, 223 (1978).
[3] F. Wilczek, Phys. Rev. Lett. **40**, 279 (1978).
[4] G. Mangano, G. Miele, S. Pastor, T. Pinto, O. Pisanti, and P. D. Serpico, Nucl. Phys. **B729**, 221 (2005).
[5] A. Melchiorri, O. Mena, and A. Slosar, Phys. Rev. D **76**, 041303 (2007).
[6] S. Hannestad, A. Mirizzi, G. G. Raffelt, and Y. Y. Y. Wong, J. Cosmol. Astropart. Phys. 08 (2007) 015.
[7] S. Hannestad, A. Mirizzi, G. G. Raffelt, and Y. Y. Y. Wong, J. Cosmol. Astropart. Phys. 04 (2008) 019.
[8] S. Hannestad, A. Mirizzi, G. G. Raffelt, and Y. Y. Y. Wong, J. Cosmol. Astropart. Phys. 08 (2010) 001.
[9] M. Archidiacono, S. Hannestad, A. Mirizzi, G. Raffelt, and Y. Y. Y. Wong, J. Cosmol. Astropart. Phys. 10 (2013) 020.
[10] E. Giusarma, E. Di Valentino, M. Lattanzi, A. Melchiorri, and O. Mena, Phys. Rev. D **90**, 043507 (2014).
[11] S. Gariazzo, C. Giunti, and M. Laveder, J. Cosmol. Astropart. Phys. 04 (2015) 023.
[12] A. H. Guth, Phys. Rev. D **23**, 347 (1981).
[13] A. D. Linde, Phys. Lett. **108B**, 389 (1982).
[14] A. A. Starobinsky, Phys. Lett. **117B**, 175 (1982).
[15] S. W. Hawking, Phys. Lett. **115B**, 295 (1982).
[16] A. Albrecht and P. J. Steinhardt, Phys. Rev. Lett. **48** (1982) 1220.
[17] V. F. Mukhanov, H. A. Feldman, and R. H. Brandenberger, Phys. Rep. **215** (1992) 203.
[18] V. F. Mukhanov and G. V. Chibisov, Pis'ma Zh. Eksp. Teor. Fiz. **33**, 549 (1981) [JETP Lett. **33**, 532 (1981)].
[19] F. Lucchin and S. Matarrese, Phys. Rev. D **32**, 1316 (1985).
[20] D. H. Lyth and A. Riotto, Phys. Rep. **314**, 1 (1999).

[21] B. A. Bassett, S. Tsujikawa, and D. Wands, Rev. Mod. Phys. **78**, 537 (2006).
[22] D. Baumann and H. V. Peiris, Adv. Sci. Lett. **2**, 105 (2009).
[23] P. A. R. Ade *et al.* (Planck Collaboration), arXiv: 1502.02114.
[24] P. Hunt and S. Sarkar, J. Cosmol. Astropart. Phys. 01 (2014) 025.
[25] D. K. Hazra, A. Shafieloo, and T. Souradeep, J. Cosmol. Astropart. Phys. 11 (2014) 011.
[26] P. A. R. Ade *et al.* (Planck Collaboration), arXiv: 1502.01589.
[27] P. A. R. Ade *et al.* (Planck Collaboration), Astron. Astrophys. **571**, A16 (2014).
[28] P. A. R. Ade *et al.* (Planck Collaboration), Astron. Astrophys. **571**, A1 (2014).
[29] R. de Putter, E. V. Linder, and A. Mishra, Phys. Rev. D **89**, 103502 (2014).
[30] A. Lewis and S. Bridle, Phys. Rev. D **66**, 103511 (2002).
[31] A. Lewis, A. Challinor, and A. Lasenby, Astrophys. J. **538**, 473 (2000).
[32] J. Martin, C. Ringeval, and V. Vennin, Phys. Dark Univ. **5-6**, 75 (2014).
[33] N. Kitazawa and A. Sagnotti, J. Cosmol. Astropart. Phys. 04 (2014) 017.
[34] F. Fritsch and R. Carlson, SIAM J. Numer. Anal. **17**, 238 (1980).
[35] F. Fritsch and J. Butland, SIAM J. Sci. Stat. Comput. **5**, 300 (1984).
[36] D. Larson, J. Dunkley, G. Hinshaw, E. Komatsu, M. R. Nolta, C. L. Bennett, B. Gold, M. Halpern *et al.*, Astrophys. J. Suppl. Ser. **192**, 16 (2011).
[37] E. Di Valentino, E. Giusarma, M. Lattanzi, A. Melchiorri, and O. Mena, Phys. Rev. D **90**, 043534 (2014).
[38] P. A. R. Ade *et al.* (Planck Collaboration), Astron. Astrophys. **571**, A15 (2014).
[39] C. L. Bennett, D. Larson, J. L. Weiland, N. Jarosik, G. Hinshaw, N. Odegard, K. M. Smith, R. S. Hill *et al.*, Astrophys. J. Suppl. Ser. **208**, 20 (2013).
[40] C. L. Reichardt, L. Shaw, O. Zahn, K. A. Aird, B. A. Benson, L. E. Bleem, J. E. Carlstrom, C. L. Chang *et al.*, Astrophys. J. **755**, 70 (2012).
[41] S. Das, T. Louis, M. R. Nolta, G. E. Addison, E. S. Battistelli, J. R. Bond, E. Calabrese, D. C. M. J. Devlin *et al.*, J. Cosmol. Astropart. Phys. 04 (2014) 014.
[42] S. W. Allen, A. E. Evrard, and A. B. Mantz, Annu. Rev. Astron. Astrophys. **49**, 409 (2011).
[43] D. H. Weinberg, M. J. Mortonson, D. J. Eisenstein, C. Hirata, A. G. Riess, and E. Rozo, Phys. Rep. **530**, 87 (2013).
[44] E. Rozo, E. S. Rykoff, J. G. Bartlett, and A. E. Evrard, arXiv:1302.5086.
[45] P. A. R. Ade *et al.* (Planck Collaboration), Astron. Astrophys. **571**, A20 (2014).
[46] P. A. R. Ade *et al.* (Planck Collaboration), arXiv: 1502.01597.
[47] C. Heymans, E. Grocutt, A. Heavens, M. Kilbinger, T. D. Kitching, F. Simpson, J. Benjamin, T. Erben *et al.*, Mon. Not. R. Astron. Soc. **432**, 2433 (2013).
[48] G. Efstathiou, Mon. Not. R. Astron. Soc. **440**, 1138 (2014).
[49] J. Hamann, S. Hannestad, J. Lesgourgues, C. Rampf, and Y. Y. Y. Wong, J. Cosmol. Astropart. Phys. 07 (2010) 022.
[50] E. Giusarma, R. De Putter, and O. Mena, Phys. Rev. D **87**, 043515 (2013).
[51] C. Blake, E. Kazin, F. Beutler, T. Davis, D. Parkinson, S. Brough, M. Colless, C. Contreras *et al.*, Mon. Not. R. Astron. Soc. **418**, 1707 (2011).
[52] F. Beutler, C. Blake, M. Colless, D. H. Jones, L. Staveley-Smith, L. Campbell, Q. Parker, W. Saunders *et al.*, Mon. Not. R. Astron. Soc. **416**, 3017 (2011).
[53] W. J. Percival *et al.* (SDSS Collaboration), Mon. Not. R. Astron. Soc. **401**, 2148 (2010).
[54] N. Padmanabhan, X. Xu, D. J. Eisenstein, R. Scalzo, A. J. Cuesta, K. T. Mehta, and E. Kazin, Mon. Not. R. Astron. Soc. **427**, 2132 (2012).
[55] K. S. Dawson *et al.* (BOSS Collaboration), Astron. J. **145**, 10 (2013) [arXiv:1208.0022.
[56] L. Anderson *et al.* (BOSS Collaboration), Mon. Not. R. Astron. Soc. **441**, 24 (2014).
[57] B. Leistedt, H. V. Peiris, and L. Verde, Phys. Rev. Lett. **113**, 041301 (2014).
[58] J. Hamann and J. Hasenkamp, J. Cosmol. Astropart. Phys. 10 (2013) 044.
[59] M. Wyman, D. H. Rudd, R. A. Vanderveld, and W. Hu, Phys. Rev. Lett. **112**, 051302 (2014).
[60] C. Dvorkin, M. Wyman, D. H. Rudd, and W. Hu, Phys. Rev. D **90**, 083503 (2014).
[61] M. Archidiacono, N. Fornengo, S. Gariazzo, C. Giunti, S. Hannestad, and M. Laveder, J. Cosmol. Astropart. Phys. 06 (2014) 031.
[62] G. G. Raffelt, Lect. Notes Phys. **741**, 51 (2008).
[63] G. G. Raffelt, Phys. Rep. **198**, 1 (1990).